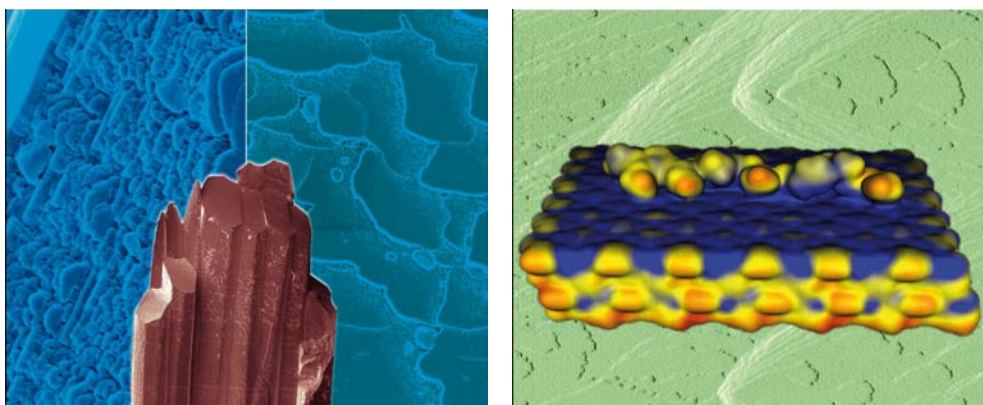


This paper is published as part of a *CrystEngComm* themed issue on:

Biom mineralisation

Guest edited by Lia Addadi
The Weizmann Institute of Science, Israel

Published in [issue 12, 2007](#) of *CrystEngComm*



Images reproduced by permission of Lia Addadi (outside) and James De Yoreo (inside)

Other papers published in this issue include:

[**Molecular dynamics simulations of the interaction of citric acid with the hydroxyapatite \(0001\) and \(01-10\) surfaces in an aqueous environment**](#)

N. H. de Leeuw and J. A. L. Rabone, *CrystEngComm*, 2007, DOI: [10.1039/b710974a](#)

[**Synthesis-dependant structural variations in amorphous calcium carbonate**](#)

Raymond S. K. Lam, John M. Charnock, Alistair Lennie and Fiona C. Meldrum, *CrystEngComm*, 2007, DOI: [10.1039/b710895h](#)

[**Calcite shape modulation through the lattice mismatch between the self-assembled monolayer template and the nucleated crystal face**](#)

Boaz Pokroy and Joanna Aizenberg, *CrystEngComm*, 2007, DOI: [10.1039/b710294a](#)

[**Fine structure of nacre revealed by solid state \$^{13}\text{C}\$ and \$^1\text{H}\$ NMR**](#)

Christian Jäger and Helmut Cölfen, *CrystEngComm*, 2007, DOI: [10.1039/b708600h](#)

Visit the *CrystEngComm* website for cutting-edge crystal engineering research

[**www.rsc.org/crystengcomm**](http://www.rsc.org/crystengcomm)

Calcite shape modulation through the lattice mismatch between the self-assembled monolayer template and the nucleated crystal face

Boaz Pokroy and Joanna Aizenberg

Received 6th July 2007, Accepted 18th September 2007

First published as an Advance Article on the web 28th September 2007

DOI: 10.1039/b710294a

The shapes of biologically formed calcite crystals are extremely versatile. Numerous studies have addressed the possible biological mechanism of crystal shape regulation. Synthetic assays have shown that the shape and morphology of calcite crystals can be modulated by inorganic or organic solution additives. Hardly any studies have to date discussed the concept of controlling the shape of these crystals by organic nucleating surfaces. We show in this paper that self-assembled monolayers (SAMs) that template calcite nucleation have two pronounced effects: in addition to inducing the highly oriented crystal growth (the phenomenon that we have extensively described in our previous studies), each SAM induces a clear modification of the calcite shape from its equilibrium rhombohedron. We demonstrate that this change in shape originates from the anisotropy of lattice mismatches that develop between the nucleating crystal face and the organic SAM in different directions. We present a model that gives qualitative predictions for the shape of crystals grown on a variety of SAM substrates, as a function of lattice mismatch, and show that these shapes correlate extremely well with the experimental results. We believe that this mechanism might be utilized by organisms in the biomineralization process.

1. Introduction

The nucleation and growth of crystals formed by organisms in the course of biomineralization are precisely controlled.^{1–3} This control is achieved by specific macromolecules, both in the form of templates and growth-modifying additives.^{1–3} The most abundant biogenic mineral is calcite, the most stable polymorph of calcium carbonate. Single calcite crystals are used in skeletons of echinoderms, foraminifera, coccoliths, and in the prisms of certain mollusk shells.^{4–10} These crystals are usually exquisitely shaped and are significantly different in their appearance from calcite rhombohedra of inorganic origin.

Several approaches have been used to gain a better understanding of the mechanisms, by which specific organic molecules exert control of crystal orientation, morphology and shape. In the first approach, calcite has been crystallized in the presence of different soluble organic molecules extracted from organisms,^{9–11} ions,¹² or synthetic polymers^{13,14} to observe their effect on crystal morphology. The second approach involves crystallization of calcite on various templates, such as Langmuir monolayers,^{15–17} functionalized polymers,^{18,19} inorganic substrates,^{20,21} biological macromolecules²² and self-assembled monolayers (SAMs),^{8,23,24} to study the effect of the substrate on crystal orientation. SAMs of alkanethiols supported on coinage metals proved to be the most flexible in their ability to nucleate well controlled and versatile crystal orientations.²⁵ SAMs form highly ordered two-dimensional crystals, which have been well characterized.²⁶ They were used as templates for controlled nucleation of

other minerals,^{23,27} semiconductors,^{28,29} organic crystals,^{30,31} and proteins.³²

Previously we have shown that a large range of nucleation faces could be observed for the growth of calcite crystals on different SAMs.²⁵ In particular, selective calcite nucleation from the (015), (104), (1.0.12), (012), (103), (107), (001),²⁵ and (113)¹² planes was induced by controlling the functional group of the SAM, parity of the alkane chain and the metal substrate. It has been demonstrated that alkanethiols self-assemble into a two dimensional crystal exhibiting a trigonal symmetry,²⁶ both on gold³³ and on silver³⁴ with lattice constants of 4.97 Å³³ and 4.77 Å³⁴ respectively. The lattice of the SAM, however, had no epitaxial effect on the orientation of the nucleated crystals. We have shown that the nucleating plane is controlled rather by the stereochemical match between the orientation of the functional groups in the SAM and the carbonate ions in calcite.^{25,35}

We have noticed that the shapes of thus oriented crystals are distorted compared to the expected equilibrium shape of the isotropic (104) calcite rhombohedron. The shape change has been also reported for the specific case of (012)-oriented calcite on SAMs.^{36,37} This result was observed despite the fact that no additives were added to the crystallization solution.

In this study we show that by calculating the anisotropic mismatch between the lattice of the SAM substrate and the lattice of the calcium ions in the nucleating plane, we can explain and predict the distortions in calcite shapes.

2. Results and discussion

In this study, we analyze the shapes of calcite crystals nucleated from the (001), (012), (015) and (104) planes. These orientations are controlled by the SAMs terminated in

School of Engineering and Applied Sciences, Harvard University,
29 Oxford Street, Cambridge, MA, 02138, USA

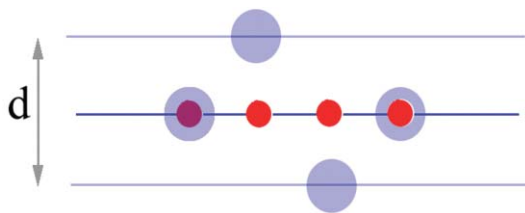


Fig. 1 Schematic presentation of the thickness, d , of the nucleation plane. The plane thickness defines the imaginary thickness of the plane that takes into account calcium ions that are slightly above and below the actual plane to keep the net-zero charge at the interface. Blue circles represent calcium ions and red circles carboxylic acid groups.

carboxylic, sulfonate and hydroxyl groups, supported on Au and Ag.²⁵ We have compared the lattice mismatch between the underlying monolayer and calcium ions in the nucleated plane. In our calculations, we assumed that calcium ions in the nucleated crystal plane form an ad-layer on the SAM. The thickness, d , of this layer is defined by the net zero charge at the interface. A schematic illustration is given in Fig. 1. In most cases described in this paper, $d = 0$. In the case of the (015) nucleating plane, we had to take into account calcium ions that are slightly above and below the actual plane and project these ions onto the surface layer. The mismatch between the SAM and the calcium array in the nucleated plane was calculated based on the known symmetry and periodicity of the monolayer,^{33,34} and calcite. Specific details for each orientation are given below.

For the majority of orientations the local symmetry of the array of calcium ions on the SAM is reduced from trigonal to triclinic. The mismatch tensor will therefore, in addition to diagonal elements, also have shear components³⁸ The general presentation is shown in Fig. 2. As mentioned above, the local symmetry of the 2D arrangement of alkanethiols on Au(111) or Ag(111) is hexagonal. In the case of alkanethiols on Au(111) and Ag(111) we chose our initial coordinate system to coincide with the a - and b -axes of the organic monolayer (Fig. 2). The angle between the identical cell parameters ($a = b$) of the monolayer is $\alpha = 60^\circ$. M_a and M_b are the mismatch vectors between the monolayer and the calcite nucleating

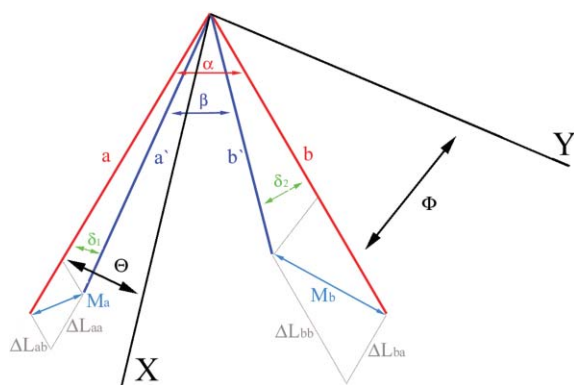


Fig. 2 Selection of the axes and schematic presentation of the relationship between the 2D lattices of the SAM and the calcium array in the nucleated plane. The red coordinates represent the SAM, while the blue one represents the calcium array of the calcite crystal.

plane: a , a' and b , b' respectively. δ_1 and δ_2 are the angles between a' , a and between b' , b respectively (see Fig. 2).

The misfit tensor can be written as follows:

$$\begin{pmatrix} \xi_{aa} & \xi_{ab} \\ \xi_{ba} & \xi_{bb} \end{pmatrix} \quad (1)$$

where:

$$\xi_{aa} = \frac{\Delta L_{aa}}{a} = \frac{a' \cos \delta_1 - a}{a} - \frac{a' \sin \delta_1}{a \cdot \tan \alpha} \quad (2)$$

$$\xi_{ab} = \frac{\Delta L_{ab}}{a} = \frac{a' \sin \delta_1}{a \cdot \sin \alpha} \quad (3)$$

$$\xi_{bb} = \frac{\Delta L_{bb}}{b} = \frac{b' \cos \delta_2 - b}{b} - \frac{b' \sin \delta_2}{b \cdot \tan \alpha} \quad (4)$$

$$\xi_{ba} = \frac{\Delta L_{ba}}{b} = \frac{b' \sin \delta_2}{b \cdot \sin \alpha} \quad (5)$$

The definitions of ΔL_{aa} , ΔL_{bb} , ΔL_{ab} , ΔL_{ba} are presented in Fig. 2.

Once we know all the components of the misfit tensor in the initial coordinate system, we transform our coordinate system to new axes: X and Y . Both X and Y always lie within the nucleating plane. X and Y are chosen in each case according to the misfit direction needed for growth rate calculations. This means we rotate the original b -axis by Φ and the a -axis by θ (see Fig. 2). The misfit tensor in the new coordinate system can be calculated using the known relationship:

$$\xi'_{ij} = a_{im} a_{jk} \xi_{km}, \quad (6)$$

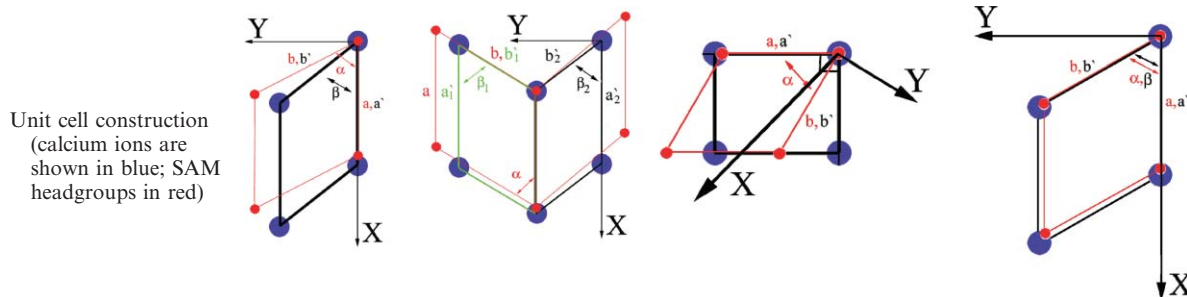
a_{im} and a_{jk} are the cosines between the i, m and j, k axes respectively.

In general, X and Y axes are chosen to be perpendicular to each other with the X -axis along the direction of the lattice match. For example, it has been shown for the SAM on gold that the a -axis of the templated calcite is lattice-matched and aligned with the a -axis of the monolayer.²⁴ This direction is then chosen as X . The construction of the array of calcium ions on the different calcite nucleation planes $\{(001), (012), (015), (104)\}$, the parameters of the templating SAM and the corresponding directions of the axes are shown in Table 1. All our calculations are based on the calcite model in which $a = 4.991 \text{ \AA}$ and $c = 17.064 \text{ \AA}$.³⁹ Using the equations formulated above, the lattice mismatch along the SAM's a, b and new X, Y axes were calculated and summarized in Table 1.

We anticipated that the observed anisotropy of the lattice mismatch between the SAM and the nucleated crystal, and the related anisotropy of the induced strain ($\epsilon_{xT}, \epsilon_{yT}$), will affect the crystal growth rates in different crystallographic directions. As a result, an anisotropic change in calcite rhombohedron shape should be expected. In order to evaluate the effect of lattice mismatch on the shape of the overgrown crystals, we choose to modify the theory of Wulff⁴⁰ and Born.⁴¹ Wulff in 1901 demonstrated that there is a ‘‘Wulff’’ point within the crystal from which the distances to the different facets are

Table 1 Anisotropy of the lattice mismatch between the SAM and the nucleated crystal plane

Nucleating plane	(012)	(012)	(015)	(104)	(001)	(001)
SAM ^a	CO ₂ ⁻ /Au(111)	CO ₂ ⁻ /Ag(111)	CO ₂ ⁻ /Au(111) ^b	OH/Au(111)	SO ₃ ⁻ /Au(111)	SO ₃ ⁻ /Ag(111)
<i>a</i> /Å	4.97	4.77	4.97	4.97	4.77	4.97
<i>b</i> /Å	4.97	4.77	4.97	4.97	4.77	4.97
<i>a'</i> /Å	4.991	4.991	4.99	4.99	4.99	4.99
<i>b'</i> /Å	4.991	4.049	4.21	3.82	4.99	4.05
α /°	60	60	60	60	60	60
β /°	51.95	51.95	60	51.95	60	90
δ_1 /°	0	0	0	0	0	0
δ_2 /°	8.05	8.05	0	8.05	0	-30
ξ_{aT} (%)	-12.75	9.09	0.42	12.85	0.42	4.63
ξ_{bT} (%)	-25.92	-22.81	-15.25	-30.10	0.37	4.01
θ /°	0	0	0	0	0	50.95
Φ /°	30	30	0	30	0	69.05
$\varepsilon_{XT}\varepsilon_{YT}$	0.57	0.46	0.56	2.76	1.13	1.15



^a SAM is abbreviated as “functional group” / “metal substrate”. ^b Calcium ions that are 1.339 Å above and below the (015) plane are taken into account in the construction of the calcium ion array in the (015) plane to maintain equilibrium of charge (see text for details). As a result the calcium ion array on the reconstructed (015) plane forms two different alternating parallelograms (left and right column), both contributing to the final strain.

proportional to the specific surface free energy. This means that the surface area of a crystal face decreases in general with increasing surface free energy, or that a crystal grows faster perpendicular to a surface with a high surface energy. Later Born in 1923 in his lattice theory demonstrated that the surface free energy can be replaced by the surface energy ($R \propto \gamma$). Hartman and Perdok⁴² in 1955 introduced the attachment energy (E_{att})⁴³ and demonstrated that for low supersaturations the relative growth rate of a face in an unstrained case (index 0) is proportional to E_{att} .⁴⁴ $R_{(hkl)} \propto E_{att(hkl)}$.

In the case of the strain, the change in the growth rate from the unstrained case $\Delta R_{(hkl)1}$ will be proportional to the strain energy perpendicular to the (hkl) plane, $E_{e\perp(hkl)}$. This is based on a small modification of the Wulff–Born construction ($R_{(hkl)} \propto \gamma_{(hkl)} - E_{e\perp(hkl)}$).

$$E_{e\perp(hkl)} = \frac{Ed\varepsilon_{\perp(hkl)}^2}{(1-\nu)} \quad (7)$$

where E is the Young’s modulus, d the layer thickness, ε the strain and ν is the Poisson ratio. The ratio between the growth rates perpendicular to two crystallographic planes will be:

$$\frac{\Delta R_{(hkl)1}}{\Delta R_{(hkl)2}} = \left(\frac{\varepsilon_{\perp(hkl)1}}{\varepsilon_{\perp(hkl)2}} \right)^2 \quad (8)$$

In order to visualize the strain effect on the shape of the crystals according to our model, we used the SHAPE 6.0[®] program (<http://www.shapesoftware.com/>). This program has

the ability to change the rate of growth of different faces. By giving a relative growth rate to each of the six equivalent cleavage (104) faces of calcite we could reconstruct the expected anisotropy (or reduction in symmetry) of the shapes of the differently oriented calcite crystals. Fig. 3 presents the results. For a better visualization of the effect, we show the shape of the undistorted crystal (left, blue), the shape of the reconstructed crystal that is affected by the mismatch strains and grows anisotropically according to our model (middle, red), and the scanning electron micrograph of the corresponding experimental system (right). It is obvious that the shape of the crystals is strongly affected by a rather slight anisotropy in growth rate. The calculations correspond well with the experimental data. The crystals appear elongated in the direction of the lattice match.

For the case of the (001)-oriented calcite on Ag and Au, we observe a very interesting phenomenon. Though the shape does not change a great deal due to the mismatch effect, one observes a very pronounced difference in the contact area of the calcite nucleating face and the SAM substrate (Fig. 4). One should keep in mind that for both cases (SAMs on Au and on Ag) the functional end group is the same. The difference between these two cases is the magnitude of the lattice mismatch along the a and b axes. In the case of the SAMs on Ag the misfits are much higher than for those on Au (see Table 1). This means that the higher the misfit in the nucleating plane the higher is the energy required for growing this plane, or in other words, the strain energy contributes to a

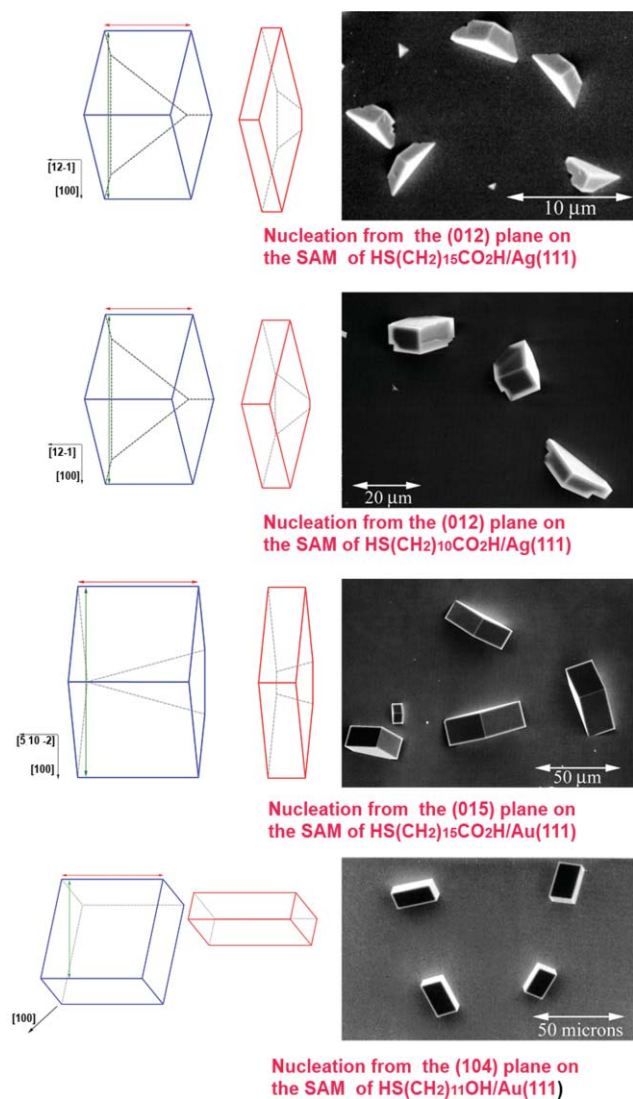


Fig. 3 Comparison of the shapes of calcite crystals grown in different orientations with and without strain. Left column: theoretical isotropic shapes reconstructed using the SHAPE program (blue). The crystal lengths A (red) and B (green) that were used for determining the extent of shape anisotropy are shown. Center: calculated anisotropic shapes that develop as a result of mismatch strains at the interface and that are reconstructed using the SHAPE program (red). Right column: scanning electron micrographs (SEM) of calcite crystals—experimental results. (a) Calcite nucleated from the (012) plane grown on $\text{HS}(\text{CH}_2)_{15}\text{CO}_2\text{H}/\text{Ag}(111)$. (b) Calcite nucleated from the (012) plane grown on $\text{HS}(\text{CH}_2)_{10}\text{CO}_2\text{H}/\text{Ag}(111)$. (c) Calcite nucleated from the (015) plane grown on $\text{HS}(\text{CH}_2)_{15}\text{CO}_2\text{H}/\text{Au}(111)$. (d) Calcite nucleated from the (104) plane grown on $\text{HS}(\text{CH}_2)_{11}\text{OH}/\text{Au}(111)$.

higher value of the surface energy. As a result the crystal will prefer to minimize the surface of the energetically higher interface by a smaller calcite/monolayer contact area. Explaining these results by the Wulff theory is also easy: The higher the surface energy of the nucleating plane the faster the crystal will grow perpendicularly, and as a consequence the surface area is minimized. This is exactly what is observed in our experiments. In order to have an intermediate case we grew calcite crystals on the same SAMs as to maintain the

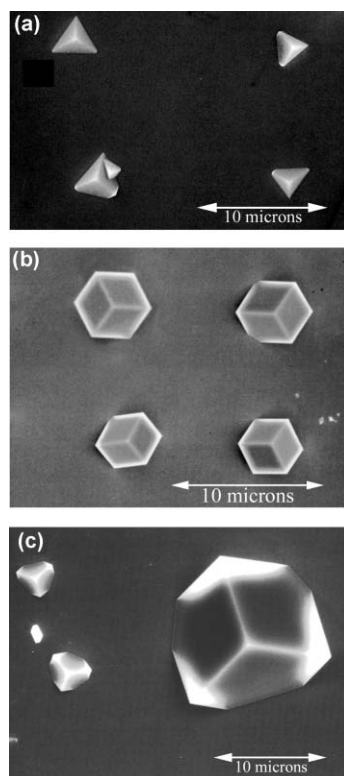


Fig. 4 SEM images of (001)-oriented calcite crystals grown on different SAM-substrate combinations: (a) $\text{HS}(\text{CH}_2)_{11}\text{SO}_3\text{H}/\text{Au}(111)$. (b) $\text{HS}(\text{CH}_2)_{11}\text{SO}_3\text{H}/\text{Ag}(111)$. (c) $\text{HS}(\text{CH}_2)_{11}\text{SO}_3\text{H}/\text{AgAu}(111)$.

same orientation, however on an alloy of silver enriched with several percent of gold (silver and gold form a solid solution⁴⁵). This case shows very clearly that when the lattice mismatch is intermediate between the cases of SAMs on pure gold or silver the contact surface is also intermediate (Fig. 4c). This change of shape can also be modeled by giving two different growth rates perpendicular to the substrate (Fig. 5a and 5b). The difference in the contact area with the surface is different for these two cases, very similar to the experimental results in Fig. 4a and 4b.

It is important to discuss here that in some cases Table 1 presents very large values for the lattice mismatch. We would like to point out that in previous investigations of oriented growth of inorganic crystals on other inorganic crystals it has been shown that surprisingly very large mismatches of up to 50% still induced epitaxial oriented growth.⁴⁶ It is clear, however, that bulk crystals cannot withstand such large lattice misfits in the form of strains. One should keep in mind that calcite is a stiff ceramic material with a Young's modulus of 78 GPa.⁴⁷ Nevertheless, the first monolayer of calcite can be significantly different from its bulk structure and withstand very high misfits. After a critical thickness the resulting distortion would attenuate completely.

Obviously, the monolayer is significantly softer than the calcite crystal, and therefore a large part of the misfit should be expected to be retained in the self-assembled organic monolayer in the form of lattice distortions (note that this latter concept has never been shown experimentally). There are

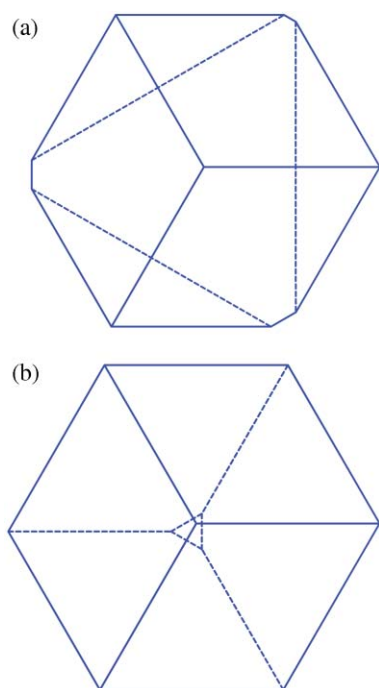


Fig. 5 Shapes of the (001)-oriented crystals reconstructed using SHAPE program. The plane of nucleation (triangle) is presented by dotted lines. (a) Calcite (001) grown on HS(CH₂)₁₁SO₃H/Au(111). (b) Calcite (001) grown on HS(CH₂)₁₁SO₃H/Ag(111).

hardly any studies that have measured the Young's modulus of SAMs. Moreover, none have given an estimate to the modulus perpendicular to the alkane monolayer chain. Along the chain, estimates of 20–50 GPa have been made.^{48,49} In order to derive an estimate for the transverse modulus we can compare SAMs to a single crystal of polyethylene. In both cases the chain is composed of linear CH₂ groups, and the interaction between the chains is primarily attractive van der Waals forces. In the case of polyethylene the modulus along the chain, E_l varies in the literature between 235 GPa and 155 GPa.⁵⁰ The transverse modulus, E_t of polyethylene varies between 1.9 GPa and 5 GPa.^{50,51} This gives a ratio between the longitudinal and transverse modulus between 50 and 135. If we apply the same ratio to the SAM, we can estimate E_t to be between 0.2 GPa and 0.55 GPa. Another way of making the estimate to E_t is by taking into account that the elastic modulus is proportional to the bond strength. The higher the bond strength the higher the elastic modulus. The CH₂–CH₂ bonds along the alkyl chain have a bond energy of about 350 kJ mol⁻¹ while the inter chain interactions of the alkythiols is about 1 kJ mol⁻¹ per CH₂ group.⁵² This coincides with our previous evaluation of the modulus perpendicular to the alkyl chains.

These values are fairly low and make the monolayer in the nucleating plane reasonably compliant. This latter point implies that a great part of the mismatch can definitely be retained by the organic monolayer. If the strain buildup in the calcite crystal is too large it would be accommodated by defects and the strain would be relaxed. The highest possible strain buildup in the crystals is on the order of 0.2%. We believe, however, that the interfacial misfit strain would affect

the shape of the entire, bulk crystal. Such influence is based on the necessity of every crystal layer added at the interface to match the underlying SAM substrate. This intersection with the substrates will constrain the overall shape. Moreover, it is also feasible that the nucleus of each crystal that nucleated on the substrate had a much more pronounced anisotropic shape with the longer dimension along the matched crystallographic direction. This shape gets “smoothened” as the crystal grows, but would never become completely isotropic.

Another experiment we performed so as to elucidate the role of the organic monolayer on the mismatch strain buildup was to grow calcite crystals with the same orientation on similar SAMs but with a different chain length. Specifically, we grew calcite crystals on carboxylic acid terminated SAMs supported on Ag using alkanethiols with 10 and 15 methylene groups in the chain. These two monolayers induce oriented growth of calcite from the (012) plane. We found that in the case of the shorter alkanethiols the crystals were less anisotropic in shape and showed higher deviation ($\left(\frac{A}{B}\right)_{C10} = 2.471 \pm 0.796$) than

crystals grown on the longer SAM ($\left(\frac{A}{B}\right)_{C15} = 3.708 \pm 0.644$) (Table 2). We believe that these results can be explained by the increased stiffness of the SAM composed of the longer molecules. As was mentioned above, the inter chain interactions of the alkythiols is about 1 kJ mol⁻¹ per CH₂ group.⁵² This means that longer chains will lead to a less deformable monolayer. As a consequence, one would expect to observe a higher anisotropy of shape in the latter case, in agreement with our results. It is important to bear in mind that if we assume a continuous interface between the SAM and the calcite crystals, then alkanethiols on the edges will have to be increasingly tilted as this interface grows larger and, eventually, be loaded in tension along the covalent chains rather than in lateral compression. This effect will limit the size of a defect-free interface between SAM and calcite. To account for this effect, we propose that the monolayer at the crystal interface is composed of small lattice-matching, defect-free domains of tilted molecules, between which missing rows of ions are added in the crystal to accommodate the lattice mismatch with the next domain. The strain in the system will be then effectively relaxed at the domain boundaries. We are currently developing this hypothesis and will report the results elsewhere.

Our results show that when crystals are induced to nucleate from any (*hkl*) plane other than (001) plane, the anisotropy of the mismatch strains in the nucleation plane will lead to a reduction in the shape symmetry of the grown crystals. Though the symmetry-related planes should have identical attachment energies and equal surface interactions with the crystallization solution they would exhibit dissimilar growth rates due to the anisotropy of the mismatch strains. A similar

Our results show that when crystals are induced to nucleate from any (*hkl*) plane other than (001) plane, the anisotropy of the mismatch strains in the nucleation plane will lead to a reduction in the shape symmetry of the grown crystals. Though the symmetry-related planes should have identical attachment energies and equal surface interactions with the crystallization solution they would exhibit dissimilar growth rates due to the anisotropy of the mismatch strains. A similar

Table 2 The extent of the anisotropy of crystal shapes

Nucleation plane – substrate	$A'/B' \pm \sigma$	A_0/B_0^a
(012) – Ag (111)/C15-COOH	3.71 ± 0.6	1.94
(012) – Ag (111)/C10-COOH	2.47 ± 0.7	1.94
(015) – Au (111)/C15-COOH	2.95 ± 0.6	1.58
(104) – Au (111)/C11-OH	1.78 ± 0.3	1.03

^a A/B ratio for the undistorted crystal.

phenomenon, morphological symmetry reduction, induced by biological molecules, was found in biogenic calcite crystals.⁶

Recently Li and Estroff³⁷ have shown that when calcite crystals grow on SAMs in a hydrogel, the anisotropy in the crystal shape (for the (012)-orientation case) weakens, and has some correlation with the hydrogel concentration. The authors suggested that this effect is due to incorporation of the agarose-gel fibers into the calcite crystals. Our model provides a different explanation for this effect: when the calcite crystals grow within the gel they have to overcome an increasing hydrostatic pressure caused by the hydrogel. This pressure increases with the volume of the crystal, hinders the anisotropic effect caused by the substrate/crystal lattice misfit and leads to lower anisotropy in the shape.

We believe that template assisted control of crystal shape induced by the anisotropy of the interfacial strains could be yet another mechanism utilized by organisms to control the shapes of the inorganic crystals in the course of biomineralization. We can speculate that one feasible example might be presented by the basic building blocks of bone—the plate-shaped crystallites of hydroxyapatite. These platelets grow within a collagenous framework and are only a few hundreds of angstroms long and wide and about 20–30 Å thick.^{53,54} Our model of controlling crystal shape by the anisotropy of the substrate/crystal misfit strains could provide the explanation for the reduction of apatite crystallite symmetry and their preferential growth in the form of platelets. It is also conceivable that the anisotropic lattice strains found in biogenic aragonite^{55,56} and calcite⁵⁷ are the result of the anisotropic strain buildup at the organic/inorganic interface. These anisotropic lattice strains, in turn, may also have an influence on the crystal shapes, so that the crystal growth is retarded in the direction of the strain.

3. Conclusions

We have shown that SAMs, as templates for calcite nucleation, induce two effects: they control the crystal orientation and modulate the crystal shape. We provide a hypothesis that the change in the crystal shape from its rhombohedral symmetry occurs due to the anisotropy of the lattice mismatch strains between the SAM and the nucleated crystal plane. The calculations of the mismatch strains and the reconstruction of the crystal shape based on the strain-induced differences in the growth rates supported the hypothesis. The simulated crystal shapes are impressively similar to the experimentally grown calcite crystals. Our study provides a new, interesting concept—the influence of the mismatch strains at the organic/inorganic interfaces on the shape of the templated crystals. We believe that this mechanism might be utilized by organisms in the biomineralization process and that it can be further employed by man to finely tune the shapes of templated crystals by the mismatch engineering at the organic/inorganic interface.

Acknowledgements

We would like to thank Prof. E. Zolotoyabko and Dr A. A. Chernov for very helpful discussions. B.P. would like to extend his gratitude to the Fulbright Visiting Scholar Program for

financial support. This work was partially supported by the Office of Naval Research (ONR) Award #N00014-05-1-0909. J.A. is the incumbent of the Gordon McKay Professor of Materials Science chair and the Susan S. and Kenneth L. Wallach Professor chair.

References

- 1 S. Weiner and L. Addadi, *J. Mater. Chem.*, 1997, **7**, 689–702.
- 2 H. A. Lowenstam and S. Weiner, *On biomineralization*, Oxford University Press, New York, 1989.
- 3 S. Mann, *Biomineralization: principles and concepts in bioinorganic materials*, Oxford University Press, Oxford, 2001.
- 4 Y. Politi, Y. Levi-Kalisman, S. Raz, F. Wilt, L. Addadi, S. Weiner and I. Sagi, *Adv. Funct. Mater.*, 2006, **16**, 1289–1298.
- 5 F. H. Wilt, *Dev. Biol.*, 2005, **280**, 15–25.
- 6 J. Aizenberg, J. Hanson, T. F. Koetzle, L. Leiserowitz, S. Weiner and L. Addadi, *Chem.–Eur. J.*, 1995, **1**, 414–422.
- 7 S. Albeck, L. Addadi and S. Weiner, *Connect. Tissue Res.*, 1996, **35**, 419–424.
- 8 J. Aizenberg, *J. Chem. Soc., Dalton Trans.*, 2000, 3963–3968.
- 9 A. Berman, J. Hanson, L. Leiserowitz, T. F. Koetzle, S. Weiner and L. Addadi, *J. Phys. Chem.*, 1993, **97**, 5162–5170.
- 10 J. M. Didymus, P. Oliver, S. Mann, A. L. Devries, P. V. Hauschka and P. Westbroek, *J. Chem. Soc., Faraday Trans.*, 1993, **89**, 2891–2900.
- 11 J. Aizenberg, J. Hanson, M. Ilan, L. Leiserowitz, T. F. Koetzle, L. Addadi and S. Weiner, *FASEB J.*, 1995, **9**, 262–268.
- 12 Y. J. Han, L. M. Wysocki, M. S. Thanawala, T. Siegrist and J. Aizenberg, *Angew. Chem., Int. Ed.*, 2005, **44**, 2386–2390.
- 13 T. P. Wang, M. Antonietti and H. Colfen, *Chem.–Eur. J.*, 2006, **12**, 5722–5730.
- 14 L. A. Gower and D. A. Tirrell, *J. Cryst. Growth*, 1998, **191**, 153–160.
- 15 E. M. Landau, M. Levanon, L. Leiserowitz, M. Lahav and J. Sagiv, *Nature*, 1985, **318**, 353–356.
- 16 E. Lose, E. Diaz-Marti, A. Zorbakhsh and F. C. Meldrum, *Langmuir*, 2003, **19**, 2830–2837.
- 17 B. R. Heywood and S. Mann, *Adv. Mater.*, 1994, **6**, 9–20.
- 18 S. Feng and T. Bein, *Science*, 1994, **265**, 1839–1841.
- 19 A. Berman, D. J. Ahn, A. Lio, M. Salmeron, A. Reichert and D. Charych, *Science*, 1995, **269**, 515–518.
- 20 B. Pokroy and E. Zolotoyabko, *Chem. Commun.*, 2005, 2140–2142.
- 21 I. W. Kim, R. E. Robertson and R. Zand, *Adv. Mater.*, 2003, **15**, 709–712.
- 22 L. Addadi and S. Weiner, *Proc. Natl. Acad. Sci. U. S. A.*, 1985, **82**, 4110–4114.
- 23 M. Nagtegaal, P. Stroeve and W. Tremel, *Thin Solid Films*, 1998, **329**, 571–575.
- 24 A. M. Travaille, J. J. J. M. Donners, J. W. Gerritsen, Najm Sommerdijk, R. J. M. Nolte and H. van Kempen, *Adv. Mater.*, 2002, **14**, 492.
- 25 J. Aizenberg, A. J. Black and G. H. Whitesides, *J. Am. Chem. Soc.*, 1999, **121**, 4500–4509.
- 26 J. C. Love, L. A. Estroff, J. K. Kriebel, R. G. Nuzzo and G. M. Whitesides, *Chem. Rev.*, 2005, **105**, 1103–1169.
- 27 B. J. Tarasevich, C. C. Chusuei and D. L. Allara, *J. Phys. Chem. B*, 2003, **107**, 10367–10377.
- 28 P. Jiang, Z. F. Liu and S. M. Cai, *Langmuir*, 2002, **18**, 4495–4499.
- 29 A. L. Briseno, J. Aizenberg, Y. J. Han, R. A. Penkala, H. Moon, A. J. Lovinger, C. Kloc and Z. A. Bao, *J. Am. Chem. Soc.*, 2005, **127**, 12164–12165.
- 30 A. Y. Lee, A. Ulman and A. S. Myerson, *Langmuir*, 2002, **18**, 5886–5898.
- 31 J. F. Kang, J. Zaccaro, A. Ulman and A. Myerson, *Langmuir*, 2000, **16**, 3791–3796.
- 32 T. Pham, D. T. Lai, D. Ji, W. Tuntiwechapikul, J. M. Friedman and T. R. Lee, *Colloids Surf., B*, 2004, **34**, 191–196.
- 33 R. G. Nuzzo, L. H. Dubois and D. L. Allara, *J. Am. Chem. Soc.*, 1990, **112**, 558–569.
- 34 P. E. Laibinis, G. M. Whitesides, D. L. Allara, Y. T. Tao, A. N. Parikh and R. G. Nuzzo, *J. Am. Chem. Soc.*, 1991, **113**, 7152–7167.

- 35 Y. J. Han and J. Aizenberg, *Angew. Chem., Int. Ed.*, 2003, **42**, 3668–3670.
- 36 A. M. Travaille, E. G. A. Steijven, H. Meeke and H. van Kempen, *J. Phys. Chem. B*, 2005, **109**, 5618–5626.
- 37 H. Y. Li and L. A. Estroff, *J. Am. Chem. Soc.*, 2007, **129**, 5480–5483.
- 38 D. Shilo, E. Lakin and E. Zolotoyabko, *Phys. Rev. B: Condens. Matter Mater. Phys.*, 2001, 6320.
- 39 E. N. Maslen, V. A. Streltsov and N. R. Streltsova, *Acta Crystallogr., Sect. B: Struct. Sci.*, 1993, **49**, 636–641.
- 40 G. Wulff, *Z. Krystallogr. Mineral.*, 1901, **34**, 449–530.
- 41 M. Born, *Atomtheorie des festen zustandes*, Teubner, Leipzig, 1923.
- 42 P. Hartman and W. G. Perdok, *Acta Crystallogr.*, 1955, **8**, 49–52.
- 43 Z. Berkovitchyellin, *J. Am. Chem. Soc.*, 1985, **107**, 8239–8253.
- 44 P. Hartman and P. Bennema, *J. Cryst. Growth*, 1980, **49**, 145–156.
- 45 O. J. Kleppa, *Acta Metall.*, 1960, **8**, 804–806.
- 46 M. Smollett and M. Blackman, *Proc. Phys. Soc. Sect. A*, 1951, **64**, 683–691.
- 47 M. E. Broz, R. F. Cook and D. L. Whitney, *Am. Mineral.*, 2006, **91**, 135–142.
- 48 V. B. Engelkes and C. D. Frisbie, *J. Phys. Chem. B*, 2006, **110**, 10011–10020.
- 49 J. I. Siepmann and I. R. McDonald, *Phys. Rev. Lett.*, 1993, **70**, 453–456.
- 50 G. D. Barrera, S. F. Parker, A. J. Ramirez-Cuesta and P. C. H. Mitchell, *Macromolecules*, 2006, **39**, 2683–2690.
- 51 T. Nishino, H. Miyazaki and K. Nakamae, *Rev. Sci. Instrum.*, 2002, **73**, 1809–1812.
- 52 O. M. Magnussen, B. M. Ocko, M. Deutsch, M. J. Regan, P. S. Pershan, D. Abernathy, G. Grubel and J. F. Legrand, *Nature*, 1996, **384**, 250–252.
- 53 S. Weiner and W. Traub, *FASEB J.*, 1992, **6**, 879–885.
- 54 S. Weiner and H. D. Wagner, *Annu. Rev. Mater. Sci.*, 1998, **28**, 271–298.
- 55 B. Pokroy, J. P. Quintana, E. N. Caspi, A. Berner and E. Zolotoyabko, *Nat. Mater.*, 2004, **3**, 900–902.
- 56 B. Pokroy, A. N. Fitch, P. L. Lee, J. P. Quintana, E. N. Caspi and E. Zolotoyabko, *J. Struct. Biol.*, 2006, **153**, 145–150.
- 57 B. Pokroy, A. N. Fitch, F. Marin, M. Kapon, N. Adir and E. Zolotoyabko, *J. Struct. Biol.*, 2006, **155**, 96–103.



Save valuable time searching for that elusive piece of vital chemical information.

Let us do it for you at the Library and Information Centre of the RSC.

We are your chemical information support, providing:

- Chemical enquiry helpdesk
- Remote access chemical information resources
- Speedy response
- Expert chemical information specialist staff

Tap into the foremost source of chemical knowledge in Europe and send your enquiries to

library@rsc.org

RSCPublishing

www.rsc.org/library